RSC Advances

PAPER

View Article Online
View Journal | View Issue

Cite this: *RSC Adv.*, 2015, **5**, 1366

Structural and electronic properties of transparent conducting delafossite: a comparison between the $AgBO_2$ and $CuBO_2$ families (B = Al, Ga, In and Sc, Y)

M. F. Iozzi,*[a] P. Vajeeston,[a] R. Vidya,[a] P. Ravindran[ab] and H. Fjellvåg[a]

The Ag-based delafossite transparent conducting oxides (TCO) are potential p-type materials for transparent electronics. However, they have attracted less attention compared with the Cu-based delafossite systems due to their difficult synthetic chemistry and relatively low conductivity. We present here a complete comparison of structural and electronic properties of these two families based on the results obtained from the periodic density functional calculation. The equilibrium structural parameters are obtained with the Perdew Burke Ernzerhof (PBE) exchange correlation functional in the calculation, while the electronic structure is investigated by using the screened hybrid functionals proposed by Heyd, Scuseria and Ernzerhof (HSE06). The structural stabilities of these two families of compounds are similar, being completely determined by the B-site metal ions. The density of states plots show that the valence band is relatively broader for the Ag-compounds. The Ag-4d orbitals are narrow and much lower in energy than the O p states. Therefore holes created at the oxygen site are highly localized and consequently have low mobility. The computed band gaps values are found to be in excellent agreement with the corresponding experimentally observed band gap values from optical measurements. The effective mass analysis suggests that for the Cu-compounds the conductivity follows the following trend: Sc > Ga ≈ Y > Al > In, in excellent agreement with the experimental observations. However, the calculated effective masses of the carriers suggest that the conductivity of the Ag-based compounds follows the following trend: Sc > Y > Ga > In > Al.

Received 11th December 2013
Accepted 6th November 2014

DOI: 10.1039/c3ra47531j

www.rsc.org/advances

I. Introduction

Transparent conducting oxides (TCO) combine transparency (band gap > 3.0 eV) and conductivity (carrier concentration > 10^{20} cm^{-3} and high mobility) and therefore are considered very promising candidates in applications as transparent electronic devices. To date a number of TCO displaying n-type conductivity are already in use in commercial devices (*e.g.* In_2O_3, ZnO and SnO_2). However, finding the p-type counterpart to be possibly used in a transparent n:p-type junction has been more challenging. In fact most of the metal oxides are not p-type conductors. This is because the acceptor levels are often due to an excess of oxygen and the created holes are strongly localized at the oxygen sites. Their mobility is therefore very low. In 1997, Hosono *et al.*[1] found p-type conductivity in $CuAlO_2$, a transparent oxide that crystallizes with delafossite structure. The suggested reason is that the Cu 3d states are energetically close to the O 2p levels, and as a results the Cu–O bond has a certain degree of covalency and the localization at the oxygen site is reduced. Since then a large amount of research activity has been carried out to understand and possibly enhance the conductive properties of different copper-based delafossite oxides ($CuBO_2$, B = B,[2] Al,[3–8] Ga,[3,9] In,[10,11] Sc,[9,12–18] Y,[3,9,13,14] and Cr[9,13,19,20]).

The silver-based delafossite oxides ($AgBO_2$, B = Al, Ga, In, Sc) are also transparent. Furthermore they have a wider band gap than the corresponding Cu-based compounds, and therefore can in principle guarantee transparency over a wider range of the spectrum. Nevertheless they have attracted less attention both experimentally and theoretically. This is because the synthetic chemistry of silver delafossite oxides is more difficult. Only a few Ag-based delafossite oxides have been synthesized in the form of thin films and the evaluation of the electrical conductivity of powder samples has several limitations.[21] Furthermore, experimental measurements show that the conductivity of the Ag-based delafossite oxides is lower than that of Cu-based delafossite oxides. For example, the conductivity of the undoped $CuGaO_2$ (ref. 22 and 23) is 5.6–6.3 × 10^{-3} S cm^{-1} whereas that for $AgGaO_2$ (ref. 24) is only 3.2 × 10^{-4} S cm^{-1}.

Generally low conductivity in a material is due to low mobility of the carriers and/or low carrier concentration. Nagarajan *et al.*[13] suggested that the holes in the d-manifold

[a]*Department of Chemistry, Center for Materials Sciences and Nanotechnology, University of Oslo, Box 1033 Blindern, N-0315 Oslo, Norway. E-mail: mariafio@kjemi.uio.no*

[b]*Department of Physics, Central University of Tamil Nadu, Thiruvarur-610004, Tamil Nadu, India*

have higher mobility than that in the p-manifold. Furthermore, the broad feature of the 4d bands (due to their diffuse nature) suggests that the holes in the Ag 4d bands shall have higher mobility than that in the Cu 3d bands, in contrast with the experimental observations. Kandpal *et al.*[25] investigated the crystal structure and electronic structure of three families of delafossite ABO_2 (A = Cu, Ag and Au; B = B, Al, Ga, In, Sc, Y). The authors suggested that the lower conductivity of the Ag family is due to a less favorable mixing of the Ag d states with the O p orbitals. They have also pointed out that when A = Ag and Au, the occurrence of A–A interactions can not be ruled out, especially when the B ion is small.[26] On the other hand these interactions are too small to play a role in determining the conductivity. The occurrence of Cu–Cu interactions was instead excluded in these studies.[13,25] Nevertheless, the Cu–Cu distance is expected to have an important role in determining the conductivity of Cu(I) oxides since they are polaronic[5,14,27] and holes are thought to hop from Cu to Cu.

The optical band gap of the Cu-based delafossites decreases along the group IIIA (B = Al, Ga and In) in apparent contrast with the trends displayed by many semiconductors of the same group. Nie *et al.*[28] solved this anomaly by observing that the measured gaps can not be associated to the direct band gap at Γ, since the latter is dipole forbidden. The optically measured band gap is instead associated with the direct band-gap transition at the next lowest energy in the conduction band. Sheets *et al.*[21] investigated the band gap trend in the $AgBO_2$ family both experimentally and computationally, finding the same band gap anomalies observed in the $CuBO_2$ systems.

There is a rich literature on computational studies of the Cu-based delafossites. The majority of the works are based on band structure calculations performed within the density functional theory (DFT) using the local density approximation (LDA) or the generalized gradient approximation (GGA) to account for the exchange–correlation energy. The on-site Coulombic correction ($+U$) is often added to the LDA/GGA energy in order to correct the self-interaction errors coming from the localized 3d states.[29–35] More recently, Scanlon *et al.*[34,36,37] used the screened hybrid approach as developed by Heyd, Scuseria and Ernzerhof (HSE06 (ref. 38)) to compute the structure and energetics of some Cu-based delafossites. A similar approach was used by Robertson *et al.*,[39,40] namely the hybrid functional screened-exchange local density approximation (sX-LDA[41]). Recently the GW approach[42] and the Tran–Blaha modified Becke–Johnson potential scheme[43] have been applied to predict high accurate band gaps in Cu-based TCO. On the contrary, a few computational studies of the Ag-based delafossite family have been published. Kandpal *et al.*[25] used plane wave/ultrasoft pseudopotential calculations to find the equilibrium geometries. Optimized structures were then used as input for the calculations using the Linear Muffin Tin Orbital (LMTO[44]) method to compute the electronic structures. The same approach was used in ref. 21. Moreover, the vibrational properties of $AgGaO_2$ and $CuGaO_2$ were computed by Kumar *et al.*[45] by using the density functional perturbation theory (DFPT) based on the LDA approach.

In the following we analyze the crystal structure, density of states, band-structures, charge density distribution, and carrier effective masses of the Ag-based family of delafossite $AgBO_2$ in comparison with the corresponding Cu-based systems. In both Ag- and Cu-based systems considered here the B metal will belong to either the IIIA group (Al, Ga, In) or the IIIB group (Sc, Y). As the gradient correction to the exchange correlation potential improves the binding energies, the equilibrium structural parameters are obtained at the GGA level within the Perdew Burke Ernzerhof (PBE[46]) functional using force as well as stress minimization. The optimized geometries are then used as input for the evaluation of the electronic structure at the HSE06 level. The ultimate goal is to provide a complete picture of differences and similarities in the calculated properties among these two families and to enlighten the reasons why the conductivity in the Ag-based compounds is lower.

II. Computational details

We have investigated two series of compounds, namely $CuBO_2$ and $AgBO_2$ (B = Al, Ga, In and Sc, Y). All the calculations were performed within the periodic density functional theory framework, as it is implemented in the VASP code.[47] The interaction between the core (Cu:[Ar], Ag:[Kr], Al:[Ne], Ga:[Ar], In:[Kr], Sc:[Ne], Y:[Ar] and O:[He]) and the valence electrons were described using the projector-augmented wave (PAW) method.[48,49] We have used the PBE gradient corrected functional for the exchange–correlation part of the potential for the structural optimization. Our previous calculations suggested[50] that structural parameters in oxides can be reliably predicted only by using large energy-cutoff to guarantee basis-set completeness. Hence, we have used a cut-off of 800 eV. The atoms were deemed to be relaxed when all atomic forces were less than 0.02 eV $Å^{-1}$ and the geometries were assumed to get optimized when the total energy converged to less than 1 meV between two consecutive geometric optimization step. The electronic properties were computed by using the screened hybrid functional as proposed by Heyd, Scuseria and Ernzerhof (HSE06) for the structures optimized at the PBE level. The reliability of this computational approach is discussed in the following section. If not specified differently, we used a Monkhorst–Pack 9 × 9 × 9 **k**-mesh for the structural optimization and the electronic structure studies. Band structures were computed by solving the periodic Kohn–Sham equation on ten **k**-points along each direction of high symmetry of the irreducible part of the first Brillouin zone.

A. Using PBE-optimized geometries for HSE06-electronic structure calculations

Table 1 reports the optimized structural parameters for the $AgAlO_2$ compound along with the percentage error with respect to the experimental data. As previously observed by Scanlon *et al.*,[34,36,37] the hybrid approach HSE clearly gives better structural parameters than the PBE approach. Nevertheless, the evaluation of the hybrid exchange correlation contribution to the total energy is computationally demanding and therefore

Table 1 Optimized equilibrium structural parameters for $AgAlO_2$ (2H polytype, read Section III.A for details). Values in parenthesis are the percentage errors $\left(\%(\text{Theor}) = \frac{100(\text{Theor} - \text{Exp})}{\text{Exp}}\right)$ with respect to the experimental data (ref. 58). 5 × 5 × 3 and 9 × 9 × 5 **k**-meshes were used in the HSE06 and PBE calculations, respectively

Method	HSE06	% (HSE)	PBE	% (PBE)
a (Å)	2.887	−0.31	2.915	0.65
c (Å)	12.254	0.29	12.383	1.34
A–O (Å)	2.111	0.52	2.137	1.76
Al–O (Å)	1.920	−0.26	1.937	0.62

not feasible for the structural optimization of a large number of systems, as we have done here.

It is worth noticing that the errors associated with the PBE approach are within the tolerable limit (*i.e.* below 2% as compared to the experimental value). This applies not only to the $AgAlO_2$ compound, but also to all compounds of the two series ABO_2 (Table 2). Furthermore the errors are systematically positive and higher for the *c*-axis parameter, that is along the direction parallel to the O–A–O linkage (Fig. 1). This is due to the lack of a correct evaluation of the correlation energy associated with the metals–oxygen bondings, typical for non-hybrid DFT approaches. It may be noted however that a systematic positive error represents an advantage when one wants to compare optimized geometries within one or more families of delafossite oxides.

On the other hand, band gaps computed at the PBE level are always underestimated severely as compared to the experimental values. Fig. 2 shows the Density of States (DOS) of the $AgAlO_2$. The solid and dashed curves represent respectively the HSE06 and PBE DOS plots, computed on the structures optimized at the HSE06 and PBE level of theory, respectively. Clearly the PBE model underestimates the band-gap giving a value below 2 eV, while the HSE06 energy gap between the highest occupied and the lowest unoccupied level is close to 3 eV, so in the range of the experimentally observed optical band-gap (see further discussion). Furthermore the band width of the PBE

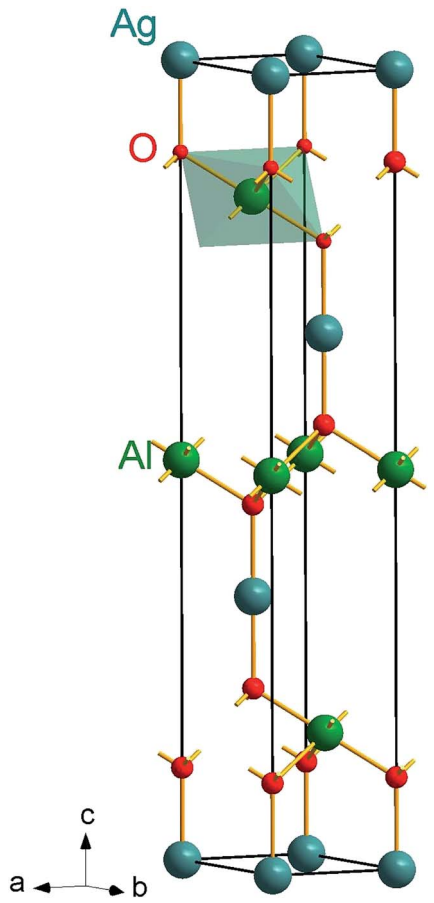

Fig. 1 $AgAlO_2$ delafossite structure (space-group $R\bar{3}m$). Silver, aluminium and oxygen atoms are shown in blue, green and red colors respectively. The structure consists of layers of slightly distorted octahedra (AlO_6) separated by the O–Ag–O linear linkage.

DOS is smaller and the PBE performance further deteriorates in describing bands well below the Fermi level. The dot-dashed curve instead shows the HSE06 DOS computed on the structure optimized at the PBE level. We will refer to this approach as PBE//HSE06. The comparison between the solid and dot-dashed

Table 2 Optimized equilibrium structural parameters for 3R form of ABO_2 (A = Ag, Cu, B = Al, Ga, In and Sc, Y). Values in parenthesis are the percentage of errors $\left(\frac{100(\text{Theor} - \text{Exp})}{\text{Exp}}\right)$ with respect to the experimental data (last column)

Compounds	*a* (Å)	*c* (Å)	A–O (Å)	B–O (Å)	Ref.
$CuAlO_2$	2.877(0.66)	17.115(0.93)	1.884(1.07)	1.923(0.68)	59 and 60
$CuGaO_2$	3.020(1.44)	17.381(1.22)	1.872(1.30)	2.022(1.30)	60
$CuInO_2$	3.359(2.03)	17.510(0.70)	1.852(0.38)	2.213(1.84)	61
$CuScO_2$	3.244(0.73)	17.221(0.71)	1.846(0.76)	2.134(0.66)	16
$CuYO_2$	3.561(0.79)	17.239(0.60)	1.835(0.44)	2.303(0.74)	60
$AgAlO_2$	2.915(0.66)	18.576	2.137(1.76)	1.937(0.62)	58[a]
$AgGaO_2$	3.038(1.64)	18.876(1.84)	2.128	2.028	62
$AgInO_2$	3.338(1.86)	19.170(1.55)	2.112(1.73)	2.210(1.66)	63
$AgScO_2$	3.241(0.93)	18.797(1.40)	2.105	2.135	62
$AgYO_2$	3.540	18.832	2.086	2.299	

[a] The experimental structure is in 2H form.

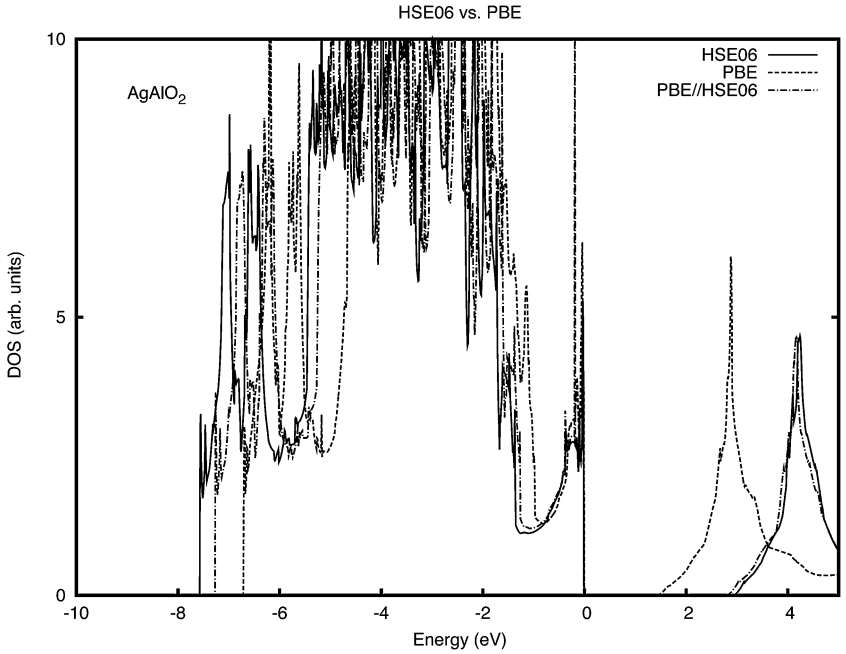

Fig. 2 Density of states of $AgAlO_2$ (2H) computed at HSE06, PBE and HSE06//PBE levels.

curve sheds light on the error introduced by taking the "expanded" PBE structure. Notably, the band-gap is only slightly lower than the one computed at the HSE06 level. Moreover the PBE//HSE06 plot mirrors the HSE06.

III. Results and discussion

A. Structural properties of ABO_2 (A = Ag, Cu, B = Al, Ga, In and Sc, Y)

All the compounds considered for the present investigation have the delafossite structure with chemical composition ABO_2. This structure consists of alternate layers of two-dimensional closed-packed A(I) ions and the slightly distorted octahedron, B(III)O_6 sharing their edges. Layers are interconnected by the linear linkage O–A(I)–O, where each oxygen atom is pseudo-tetrahedrally coordinated with one A(I) ion and three oxygen atoms. There exist two different polytypes, depending on the relative arrangement of the layers along the stacking axis. The 3R polytype has a rhombohedral symmetry, with space-group $R\bar{3}m$ and a stoichiometric unit cell (see Fig. 1). Whereas the 2H polytype has a hexagonal symmetry with space group $P6_3/mmm$ and double formula unit per unit cell. Since the two polytypes have almost the same total energies ($\Delta E(2 \times 2H - 3R) = 0.05$ eV for $AgAlO_2$) and electronic features,[51] the investigation for all the compounds were made in the 3R polytype. Optimizations started from the experimentally available 3R-structural parameters for all the compounds except $AgAlO_2$ and $AgYO_2$. In the case of $AgAlO_2$ the starting structural parameters for the 3R structure were chosen from the experimental equilibrium volume of the 2H structure. For $AgYO_2$ no experimental structural parameters were available and hence we have taken the structural parameters of $AgScO_2$ as a starting point.

Table 2 shows the optimized equilibrium structural parameters in the 3R structure for all the compounds considered in the present study. Values in parenthesis are the estimated percentage of errors with respect to the corresponding experimental structural parameters. Notice that the *a*-lattice parameter is the distance between A(I) metal ions, namely the Cu–Cu and Ag–Ag distances, while the *c*-lattice parameter is related to the interlayer stacking distance.

As the atomic number of B ions increases (Al > Ga > In > Sc > Y) the *a*-lattice and the *c*-lattice parameters increase in both series of compounds. In fact, when the B radius increases, the BO_6 octahedron becomes more bulky (B–O distance increases) inducing an enlargement of the entire structure. Surprisingly this does not correspond to an elongation of the A–O distance, that instead decreases along the group. These trends were observed and analyzed by Kandpal *et al.*[25] The authors hypothesized that, when the B ions are small, the A ions are compressed on the *ab*-plane. To minimize the repulsion some charge is pushed out of the plane and transferred to the antibonding A $d_{z^2}\cdots$O p_z states, thus weakening the A–O bond. As the B ion size increases the constrain is released in favor of a more positive bonding interaction between the A ion and the oxygen. Consequently the A–O bond distance decreases.

For a given B, the *c*-lattice parameter and the A–O distance are significantly longer in the $AgBO_2$ than in the $CuBO_2$. On the contrary the *a*-lattice parameters in the two series are quite similar thus indicating that the A–A distance is solely determined by the dimension of B and it is independent from the nature of the A-metal. This observation supports the idea that tiny or no-interaction occurs between the A-ions, even when A = Ag. It shall be noticed however that the theoretical approach used to evaluate the bonding interaction here does not take into

account relativistic and spin–orbit coupling energy contributions that instead may be relevant in such a type of contacts.

B. Analysis of electronic structure

1. Density of states (DOS). Fig. 3 shows the calculated total density of states (DOS) and site projected density of states (PDOS) for $AgAlO_2$ (lower graph) and $CuAlO_2$ (upper graph) obtained from the hybrid functional calculation using the optimized structural parameters in the PBE level. The Fermi level is set to 0 eV to have meaningful comparison. In both DOS graphs the Al states appear at the bottom of the conduction band and hence not significantly contribute to the valence band region. The valence band can be divided into three areas (namely regions I, II and III). Region I consists of hybridized A d_{z^2} and O 2p states, whereas, regions II and III are mainly dominated by the A d states and O 2p states, respectively. Clearly there are noticeable differences between the DOS plot of $AgAlO_2$ and $CuAlO_2$. In particular the total valence band DOS of $CuAlO_2$ (between −8.4 eV and 0 eV) is broader than that of $AgAlO_2$ (−7.5 eV and 0 eV). This is due to the shorter bonding interactions present in $CuAlO_2$, resulting into a wider overlap pattern of orbital states. On the other hand, the region II of $AgAlO_2$ (between −1.8 eV and −6 eV) is wider than that of the $CuAlO_2$ (between the −1.8 eV and −3.8 eV) and can be divided into two sub regions (namely regions IIa and IIb). States between −1.8 eV and −2.4 eV (region IIa) consist of O 2p states hybridized with some Ag d states, while the area between −2.4 eV and −6 eV is a strong admixture of Ag d and O 2p (IIb) character. The DOS analysis of $CuAlO_2$ in Fig. 3 shows that the region II consists mainly of Cu d states with some O 2p states.

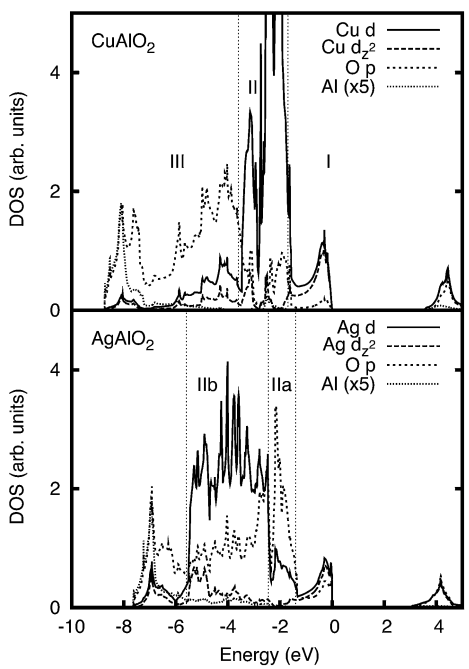

Fig. 3 The partial density of states of $AgAlO_2$ (bottom graph) and $CuAlO_2$ (top graph) in the 3R structure obtained from HSE06 functional using theoretically optimized lattice parameters.

The strong admixture of Ag d and O 2p (IIb) is mainly due the more diffuse nature of the Ag 4d orbitals which bring more overlap with the O 2p states. Furthermore, the Ag 4d bands are located deeper with respect to the top of the VB as compared to the Cu 3d. This causes the IIa region to be dominated by the O p orbitals in $AgAlO_2$. Furthermore, the overlap of the O 2p and Ag d states bring the O 2p–Ag d bonding state lower in energy resulting in low amounts of Ag-4d states present at the VBM. This testifies to the more covalent nature of the Ag–O bond as compared with the Cu–O bond (because the covalent interactions move the bonding hybrid below the VBM). Hence, the holes created in $AgAlO_2$ will have a strong component from the oxygen state. Since the holes in the p-manifold have lower mobility than the holes in the d-manifold, the conductivity of the Ag-based delafossite is expected to be lower than that of the Cu-based compounds.

Fig. 4 shows the DOS for $AgBO_2$ (left side) with B = Al, Ga, In, Sc and Y. The DOS analysis for $CuBO_2$ is also shown for comparison (right side). The main features of DOS distribution observed for $AgAlO_2$ are present also for B = Ga and In due to the isoelectronic as well as isostructural nature of these compounds. The major difference is the width of the PDOS of

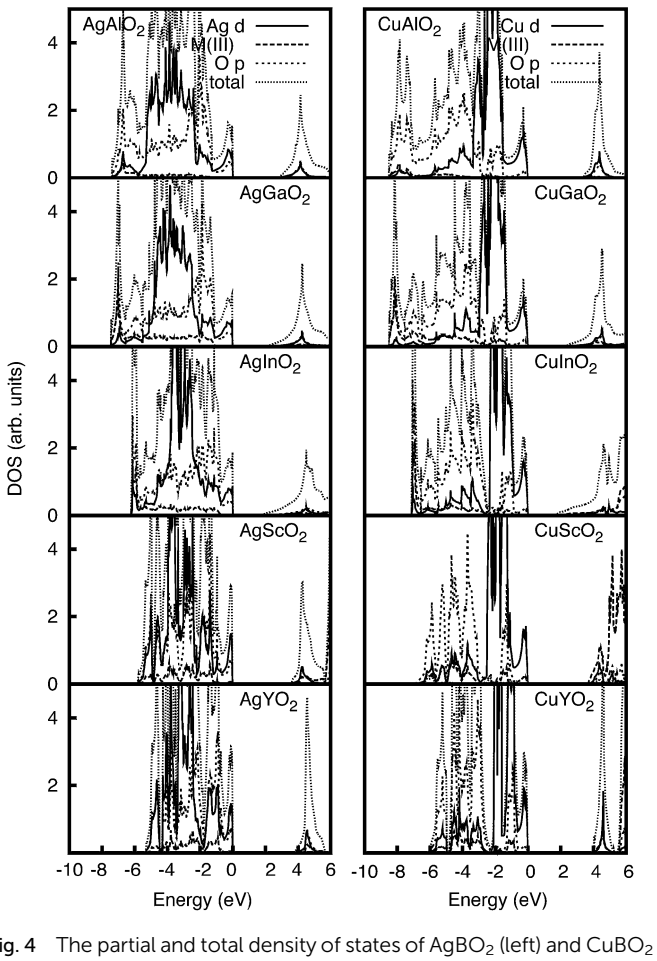

Fig. 4 The partial and total density of states of $AgBO_2$ (left) and $CuBO_2$ (right) families (B = Al, Ga, In, Sc and Y) in the 3R structure obtained from HSE06 functional using theoretically optimized lattice parameters.

Ag d states that shrinks when one goes from Al to In. In fact as the volume of the B-octahedra increase the bonding interactions shorten, resulting in a narrower bonding states distribution. This occurs also in the Cu-based delafossite, in qualitative agreement with the experimental observations.[52]

Interestingly, the PDOS of $AgBO_2$ when B = Sc and Y are significantly different from that of the $AgAlO_2$ system. Besides a small contribution from the B states, the valence band is due to the strong hybridization of Ag d and O 2p states. Since the contribution from the 4d-manifold dominates the VBM, we expect the mobility of holes to be higher for B = Sc and Y than that for B = Al, Ga, In.

2. Band structure analysis. Tables 3–5 summarize the band parameters obtained from the calculated band structures of ABO_2 compounds. In order to have more insight into the band structure of $AgBO_2$ the calculated band structures are shown in Fig. 5 and 6 and the relevant points are highlighted. We focus first on the compounds with B = IIIA elements. Like the Cu-based delafossite, the Ag-based compounds are also indirect band gap materials as evident from the depicted band structures. The valence band maximum (VBM) occurs at F point and the conduction band minimum is always at Γ point. The orbital projected band structure analysis shows that the bottom-most valence band at the F point (F_{vb}) is characterized by a strong admixture of Ag d_{z^2} and O p_z, while the top-most conduction band at the F point (F_{cb}) is characterized by Ag $p_{y/x}$, some O $p_{y/x}$ characters mixed with Al p states. The character of the top-most conduction band at the L point (L_{cb}) also have similar character as that at the F point. Going from B = Al to In in the $AgBO_2$ series, the electronic energy levels at F_{cb} and L_{cb} are pushed upward in energy. In fact, due to the volume increase, the states with charge density in the interstitial region are shown to have higher energy.[28] Therefore the direct band gap values between the F and L points increases. For $AgAlO_2$ the valence band at Γ (G_{vb}) is purely a non-bonding O $p_{y/x}$ state, while the conduction band (G_{cb}) is Ag d_{z^2} with minor contribution from s-orbitals of Ag, O and the B metal. As the radius of the B ion increases, the G_{vb} gains some contribution from B d and Ag 4d states and is therefore pushed upwards. On the other hand the anti-bonding B s levels are pushed downward and so is the G_{cb}. Consequently the direct transition at Γ and the indirect transitions decrease in energy.

Similar trends have been already observed for the Cu-compounds. The only exception is made by the direct band gap at L for the $CuGaO_2$ not following the trend, but being slightly lower than the value of $CuAlO_2$. Nie *et al.*[28] explained this irregularity by noting that the L_{cb} point contains group-III s character and that the Ga 4s has much lower energy than Al 3s orbitals. This irregularity is not present in the Ag-based family because the contribution from the group IIIA s orbital is much lower in the Ag-family as compared to the Cu-family. It is worth noting however that previous calculations[21] report the same irregularity for the direct band gap at the M point of $AgGaO_2$ (2H). However the authors in ref. 21 used the LMTO method while we are using the more accurate HSE06 approach.

For the group IIIB compounds, the Ag-based and the Cu-based families differ (Fig. 6). The $AgScO_2$ and $AgYO_2$ are still indirect band gap materials with the VBM placed at L and the CBM at Γ. This is at variance with the corresponding Cu-based compounds that in fact have a direct band gap.

Within the Ag-based family the configuration at F and L in the IIIB compounds is similar to the IIIA compounds and the fundamental direct band gap follows the same trend (increasing from Sc to Y). Interestingly the configuration at Γ_{vb} in both $AgScO_2$ and $AgYO_2$ is solely due to the non-bonding O $p_{y/x}$ state, similarly to what has been observed for $AgAlO_2$.

At Γ_{cb} instead the amount of anti-bonding B s levels decreases passing from Sc to Y and so the energy is shifted upwards. As a results the direct band gaps at Γ and the indirect band gaps increase in energy along the IIIB group.

An overview of the measured optical band gaps for the two families is given in Tables 3 and 4. The correlation between the measured optical band gaps and the calculated band gaps for the Cu-based delafossite has been already discussed elaborately. The experimental values increase along the IIIA group, 3.5 ($CuAlO_2$) → 3.6 ($CuGaO_2$) → 3.9–4.4 ($CuInO_2$), in apparent contrast with the trends displayed by many semiconductors of group IIIA. Nie *et al.*[28] observed that the measured gaps cannot be associated to the direct band gap at Γ, since the latter is dipole forbidden. The optically measured band gap is instead associated with the direct band-gap transition at the next lowest energy in the conduction band. Therefore the experimental band gaps shall be compared with the computed direct band gap at L, that in fact decreases along the group, despite the irregularity observed for the $CuGaO_2$ compound. The lower

Table 3 Comparison between the computed and experimental optical transitions for $CuBO_2$ (B = Al, Ga, In and Sc). E_g is the computed band gap, *i.e.* the energy for the transition VBM → CBM (the high symmetry points corresponding to the VBM and CBM are also indicated). E_{dir}(exp) and E_{ind}(exp) are the observed lowest direct and indirect transitions, respectively. Values are in eV

B	ΔF_{dir}	ΔL_{dir}	E_g	E_{dir}(exp)	E_{ind}(exp)
Al	4.3	4.1	3.4 ($F \rightarrow \Gamma$)	3.5 (ref. 7, 64 and 65)	3.0[a] (ref. 7, 64 and 65)
Ga	4.5	4.0	2.2 ($F \rightarrow \Gamma$)	3.6 (ref. 66)	—
In	4.7	4.5	1.6 ($F \rightarrow \Gamma$)	3.9 (ref. 54), 4.15 (ref. 11), 4.45 (ref. 67)	1.44 (ref. 67)
Sc	4.8	3.7	3.7 ($L \rightarrow \Gamma$)	3.6 (ref. 12)	—
Y	5.0	4.0	4.0 ($L \rightarrow \Gamma$)	—	—

[a] Values in the range 1.65 ÷ 2.1 eV have been originally reported as indirect transitions and lately ascribed to the presence of impurities.[7,64]

Table 4 Comparison between the computed and experimental optical transitions for $AgBO_2$ (B = Al, Ga, In and Sc). E_g is the computed band gap, *i.e.* the energy for the transition VBM → CBM (the high symmetry points corresponding to the VBM and CBM are also indicated). The experimental optical transitions have not yet been resolved into direct and indirect transitions. For the sake of clearness, the form of the samples on which the measurements were done is also reported. Values are in eV

B	ΔF_{dir}	ΔL_{dir}	E_g	E(exp)
Al	4.4	4.5	2.7 ($F \rightarrow \Gamma$)	3.6 (powder)[21]
Ga	4.5	4.6	1.8 ($F \rightarrow \Gamma$)	2.38 (crystal),[68] 2.4 (powder)[69], 4.12 (film)[24]
In	4.7	4.9	1.5 ($F \rightarrow \Gamma$)	1.9 (crystal),[68] 4.2 (film)[55]
Sc	5.0	4.2	3.4 ($L \rightarrow \Gamma$)	3.8 (powder)[21]
Y	5.1	4.4	3.7 ($L \rightarrow \Gamma$)	—

Table 5 Optical transitions computed on the basis of the calculated band structures of ABO_2 (A = Ag, Cu; B = Al, Ga, In and Sc, Y). Direct transitions ($\Delta\Sigma_{dir}$) refer to the energy difference between the highest occupied and lowest unoccupied bands at the high symmetry point Σ. Indirect transitions ($\Delta(\Sigma \rightarrow \Gamma)$) refer to the energy difference between the highest occupied band at Σ and the lowest unoccupied at Γ. Values are in eV

B	ΔF_{dir} Ag	ΔL_{dir}	$\Delta\Gamma_{dir}$	$\Delta(F \rightarrow \Gamma)$	$\Delta(L \rightarrow \Gamma)$	ΔF_{dir} Cu	ΔL_{dir}	$\Delta\Gamma_{dir}$	$\Delta(F \rightarrow \Gamma)$	$\Delta(L \rightarrow \Gamma)$
Al	4.4	4.5	4.4	2.7	3.0	4.3	4.1	5.1	3.4	3.5
Ga	4.5	4.6	3.2	1.8	2.3	4.5	4.0	3.5	2.2	2.3
In	4.7	4.9	2.4	1.5	1.9	4.7	4.5	2.5	1.6	1.7
Sc	5.0	4.2	4.7	3.7	3.4	4.8	3.7	5.6	4.1	4.0
Y	5.1	4.4	4.9	3.9	3.7	5.0	4.0	5.4	4.2	4.1

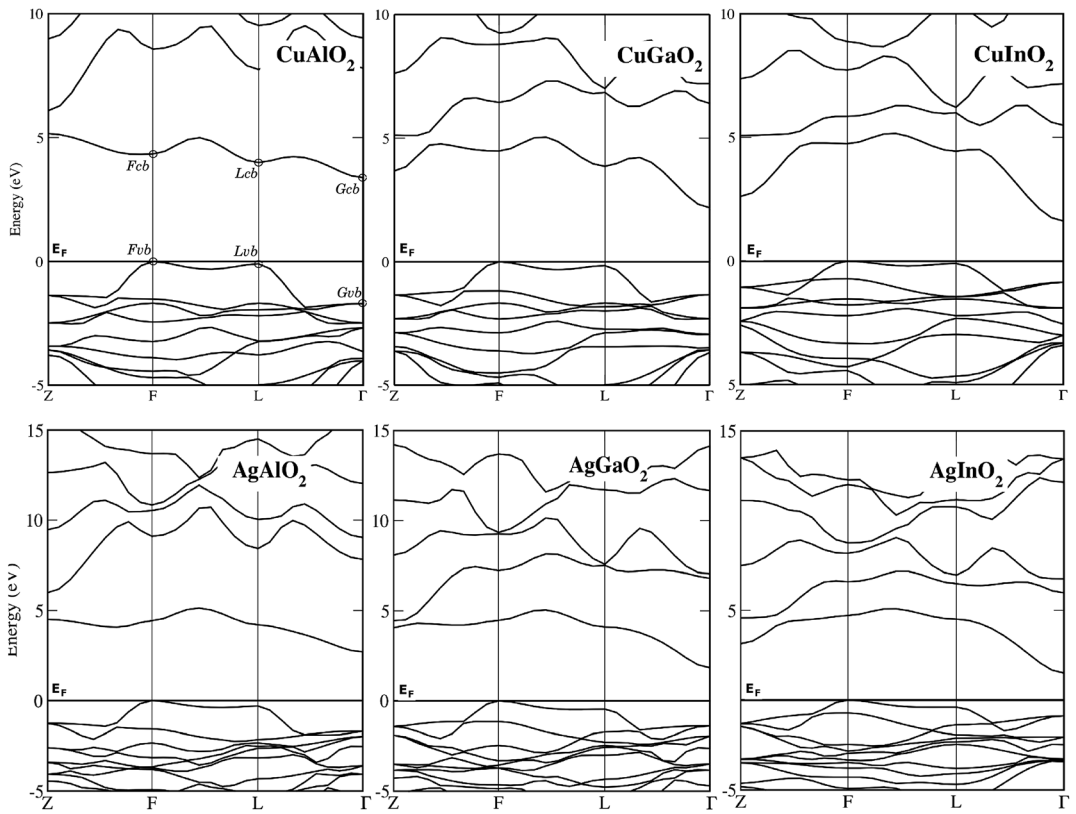

Fig. 5 Band structures of ABO_2 (A = Ag, Cu; B = Al, Ga, In).

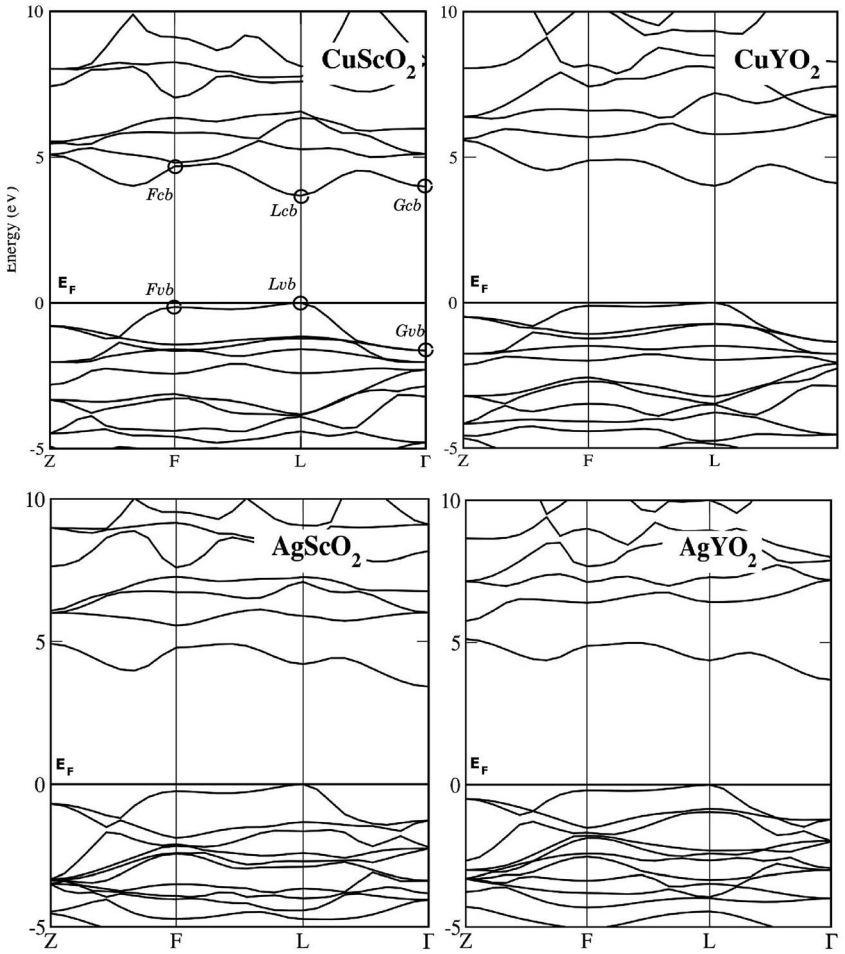

Fig. 6 Band structures of ABO_2 (A = Ag, Cu; B = Sc, Y).

optical band gaps observed for $CuAlO_2$ (1.65–2.1 eV) are likely to be due to impurities. By analogy one could postulate that the low optical absorption observed for $CuInO_2$ (1.4 eV) is due to impurities. On the contrary, our calculation shows that it shall be due to either a dipole-forbidden transition ($\Delta^{calc}\Gamma_{dir} = 2.5$ eV) partially allowed or an indirect transition ($\Delta^{calc}(F \rightarrow \Gamma) = 1.6$ eV and $\Delta^{calc}(L \rightarrow \Gamma) = 1.7$ eV).

Establishing trends in the observed optical band gaps for the Ag-compounds is more difficult since not all the experimental values are from a homogeneous set of samples. The optical band gaps for $AgAlO_2$ and $AgScO_2$ refer to samples in powder form, and they were measured by using diffuse reflectance spectroscopy which has several limitations when applied to powder samples.[21] Furthermore the measurements on thin films give higher values than those obtained from powder or single crystal samples. Nevertheless an increasing trend can be identified, namely 3.6 (Al, powder) → 4.1 (Ga, film) → 4.2 (In, film). These values compare well with the computed direct band gaps at *F*, that in fact increase along the group (4.4 (Al) → 4.5 (Ga) → 4.7 (In)). The transitions at lower energy observed for $AgGaO_2$ (2.4, powder) and $AgInO_2$ (1.9, crystal) have been interpreted by Sheets *et al.*[21] as due to the forbidden direct transition at Γ and the indirect band gaps at *F* being partially allowed. According to our calculations the computed direct band gaps at Γ are 3.2 eV ($AgGaO_2$) and 2.4 eV ($AgInO_2$) while the indirect band gaps are much lower in energy. Therefore we believe that the mentioned low energy transitions are due only to forbidden direct gaps at Γ. This also explains the reason why there are not absorptions in the visible range for the $AgAlO_2$ and $AgScO_2$. The Γ_{vb} for the latter two compounds is strongly stabilized, being solely composed by non-bonding O $p_{y/x}$ states. The forbidden direct gaps at Γ (4.4 eV (Al) and 4.7 eV (Sc)) are therefore much higher than the ones observed for $AgGaO_2$ and $AgInO_2$. The corresponding forbidden transitions are unlikely to happen and if occur, they will not be in the visible range.

C. Bader charge analysis

Table 6 shows the Bader charges for the ABO_2. We recall that the formal oxidation states for the A, B and O species are +1, +3 and −2 respectively and that Bader charges close to the formal charge indicate high degree of ionicity.

The Bader charges on the B ions are the same in the two families, indicating that the character of the B–O bond is not strongly influenced by the nature of the A metal. Interestingly there is an abrupt change in the charges passing from Al to Ga, in both the Ag-based and Cu-based families. In particular the

Table 6 Bader partial electron charges (in units of charge) for ABO_2 (A = Ag, Cu; B = Al, Ga, In and Sc, Y)

	A	B	O	A	B	O
A	Ag			Cu		
Al	+0.49	+2.46	−1.47	+0.50	+2.44	−1.47
Ga	+0.47	+1.72	−1.10	+0.55	+1.72	−1.14
In	+0.46	+1.83	−1.14	+0.54	+1.83	−1.19
Sc	+0.45	+2.02	−1.23	+0.55	+2.02	−1.28
Y	+0.41	+2.16	−1.28	+0.50	+2.16	−1.33

Table 7 Effective masses (in units of free electron mass, m_O) for ABO_2 (A = Ag, Cu; B = Al, Ga, In and Sc, Y)

	VBM	m_{100}	m_{010}	m_{001}	m_{100}	m_{010}	m_{001}
		Ag			Cu		
Al	F	0.98	0.98	0.32	1.23	1.23	0.35
Ga	F	0.87	0.87	0.28	1.23	1.23	0.33
In	F	1.05	1.05	0.31	1.85	1.85	0.40
Sc	L	1.19	0.24	1.19	1.64	0.28	1.64
Y	L	1.49	0.26	1.49	2.22	0.33	2.22

charges on O and B decrease significantly, becoming less negative and positive respectively. Therefore the Al–O bond has a higher degree of ionicity than the Ga–O bond. We speculate that this is due to the radius of the Al ion being so small to impose a compressive strain into the $AAlO_2$ structures. As noted by Kandpal some charge is then pushed into antibonding orbitals of the A–O bond, resulting in a higher charge localization on the oxygens and more polarized B–O bonds.

Besides this abrupt change there are clear trends along the groups. When the B ions radius increases, the charges on B and on the oxygen increase (in absolute value) thus indicating an increasing degree of ionicity of the B–O bond along the groups.

By comparing the Ag-based and Cu-based families, it appears clearly that the charges on the oxygen atoms are more negative in the Cu-based compounds. Furthermore charges on the Ag metal are less positive than the charges on the Cu ions for all the compounds. Therefore for a given B, the Ag–O bond has a higher degree of covalency than the Cu–O. Along the groups the Cu charge does not change significantly while the charges on Ag decrease, indicating that the Ag–O bond becomes more covalent as the B-radius increases.

D. Effective mass

To investigate the electron conduction properties we computed the hole effective mass at the valence band. The diagonal elements of the effective mass tensor m_c are classically defined according to

$$\frac{1}{m_c(\mathbf{k})} = \frac{1}{\hbar^2}\frac{\partial^2 E(\mathbf{k})}{\partial \mathbf{k}^2} \quad (1)$$

where $E(\mathbf{k})$ is the energy at the band edge. It is worth noting that the classical model relies on the assumption that the band edges are parabolic. Instead, the curvature of the top of the valence band of the delafossite TCO are very flat (see Fig. 5 and 6), making the parabolic approximation rather drastic. For a more accurate approach one shall account for non-parabolic bands and several bands contributing to the conductivity, as was done by G. Hautier *et al.*[53]

We have here computed the band edge around each high symmetry points with a set of ten **k**-points along each crystallographic direction [100], [010] and [001]. The energy regions were chosen to be small enough in **k**-space to guarantee within a certain approximation the parabolic curvature of the band edge. The band edge energies were then fitted with a ninth order polynomial fit and the second order derivative computed numerically.

The effective masses are indicative of the conductive properties of a material. For a p-type material, low effective mass corresponds to high mobility of the holes at the valence band and consequently high conductivity. Table 7 shows the effective masses at the VBM points (namely at *F* point for $AAlO_2$, $AGaO_2$ and $AInO_2$ and at *L* point for $AScO_2$ and AYO_2). The effective masses computed at the point *F* are isotropic along the [100] and [010] directions with the lowest value always obtained along the [001] direction. The effective masses at *L* are instead isotropic along the [100] and [001] directions and have the smallest value along the [010] direction. This is in agreement with the transport effective masses reported by Scanlon *et al.* for the $CuBO_2$ (B = Ga, In, Sc) compounds.[29] It is worth noting that their values are different from Table 7. This may be ascribed to the different formalism adopted by the authors $\left(\frac{1}{\hbar^2 k}\frac{dE}{dk}\right)$, the different level of theory used and the different **k**-point sampling. However, the trend remains the same.

The effective masses for the Cu-based compounds follow the trend: Sc < Ga ≈ Y < Al < In. So the conductivity follows the opposite trend: Sc > Ga ≈ Y > Al > In. This is in excellent agreement with the experimental observations. In fact the conductivity of the doped $CuInO_2$ (ref. 54) is the lowest observed among the group. The conductivity of $CuAl_{1-x}Mg_xO_2$ (ref. 23) (4×10^{-4} S cm^{-1}) is slightly above, followed by $CuY_{1-x}Ca_xO_2$ (ref. 13 and 19) (1 S cm^{-1}) and $CuGa_{1-x}Fe_xO_2$ (ref. 9) (1 S cm^{-1}). The highest conductivity has been assigned to $CuSc_{1-x}Mg_xO_2$ (ref. 9) (30 S cm^{-1}). For the Ag-based compound the effective masses follow the following trend: Sc < Y < Ga < In < Al. Therefore we postulate that the conductivity of the Ag-based delafossite TCO will follow the trend Sc > Y > Ga > In > Al. The experimentally measured conductivities of the $AgGaO_2$ (ref. 24) and $AgInO_2$ (ref. 55) thin films are 3.2×10^{-4} S cm^{-1} and 1×10^{-5} S cm^{-1}, respectively, in agreement with our hypothesis.

IV. Discussion and conclusion

By using the PBE//HSE06 computational strategy we were able to investigate ten delafossite compounds, namely ABO_2 (A = Cu and Ag; B = Al, Ga, In and Sc, Y). Our approach has been validated against pure HSE06 and experimental values and it is the best compromise between accuracy and computational feasibility.

The structures of the Ag-based delafossite materials are similar to that of the Cu-based compounds, being determined solely by the B ion. In fact for a given B, the B–O bond length and the A–A distance are similar in the Ag-based and Cu-based compounds. Instead the A–O bond length is longer in the Ag-based material leading to a crystal structure more "expanded" along the *c*-axis. As was already observed for the Cu-based, the A–O bond length decreases along the IIIA and IIIB groups. This is because the internal constrain due to the size of the B ion is released as the radius increases, in favor of a more positive bonding between the A metal and the oxygen. It is worthy to notice however that the computed Ag–O distances, ranging between 2.137 Å (B = Al) and 2.086 Å (B = Y) are very close to that observed in silver-oxides (the Ag–O bond is 2.155 Å and 2.097 Å in AgO and Ag_2O,[56] respectively). Therefore the internal constrain does not force the Ag–O moiety into an unusual bonding configuration.

It has been suggested that the character of the A–O bond plays an important role in determining the p-type conductivity of the delafossite TCOs. The occurrence of a covalent bonding between the Cu and O explains in fact the lower degree of localization and the higher mobility of the holes in $CuAlO_2$.[1] We have investigated the nature of the A–O bond *via* the Bader charge analysis, showing that for any given B the Ag–O bond is more covalent than the Cu–O bond. Furthermore the degree of covalency tends to increase as the B ion radius increases. Therefore one should in principle expect that holes created at the oxygen site would have higher mobility in the Ag-based delafossite. This is contrary to what has been experimentally observed. The degree of covalency as defined *via* the Bader charge localization techniques is therefore not a good observable to explain the different mobility of the hole created in Cu-based and Ag-based delafossite.

The major difference between the two families is the band structure composition as it appears from the PDOS analysis. The Ag 4d band in the Ag-based compounds spreads over a wider range of energies and lies lower as compared to the 3d band in the Cu-based compounds. This explains the lower mobility in the Ag-based compounds: holes created in the shallow levels (around −2 eV below the Fermi level) will have strong O p character and will be therefore strongly localized at the oxygen sites. As the B ion radius increases (B belongs to IIIA) the 4d bands are narrowed but remain always below some strongly localized O p bands. When B belongs to IIIB group, a strong Ag d/O p admixture covering the entire valence band should correspond to a higher mobility of holes.

We have computed the effective mass to rank the mobility of the holes in the different Cu-based and Ag-based delafossite materials. According to our calculations the conductivity of the Cu-based delafossite should follow the trend Sc > Ga ≈ Y > Al > In, in perfect agreement with the experimental measurements. By extension we expect the conductivity of the Ag-based delafossite to follow the trend Sc > Y > Ga > In > Al. This is not surprising since in $AgScO_2$ the shallow levels below the Fermi level (between 0 eV and −1.8 eV) present a high degree of covalent mixing of O p and Ag d states, while in $AgAlO_2$ they are due primarily to non-bonding O p states.

In conclusion, despite the fact that the Ag-based delafossite are wide band-gap materials (even wider than the corresponding Cu-based) they are not promising for the engineering of transparent electronics. Their conductivity is very low, due to the low mobility of the carriers. The low mobility is caused by the unfavorable energy match between O p and Ag 4d levels. Among the Ag-based family only $AgScO_2$ and $AgYO_2$ display a valence band configuration more suitable for p-type conductivity. Furthermore the large B ion radius makes the intercalation of oxygen more likely to occur in these compounds, increasing the amount of carriers and eventually the conductivity.

Several studies have proved that oxygen excess and metal deficit within the crystallite sites enhance the p-type conductivity in delafossite materials. Furthermore oxygen intercalation in the interstitial sites may leave empty states in the valence band, which act as holes. Therefore the defect chemistry is of primary importance as it allows the improvement of the conductivity by controlling the preparation conditions of the material. Delafossite materials with M^{III}-ions having f-orbitals have clearly larger radius than Y and should therefore display potentially higher p-type conductivity upon oxygen intercalation. In this framework one promising family of materials could be $ANdO_2$, with A = Ag and Cu. In fact the reported optical band gap for $CuNdO_2$ is 3.1 eV and the conductivity at room temperature is 2.7×10^{-2} S cm^{-1}, *i.e.* higher than that of the native $CuAlO_2$ (1.7×10^{-3} S cm^{-1}).[57] The intercalation of oxygen is likely to be facilitated by the large radius of the Nd ions, while the electronic feature of the Cu–B bonding should not be changed significantly due to the low contribution of the f-orbitals in the bonding interaction. In light of our present results we do not expect the bonding nature of the Ag–Nd bonding to be more favourable than Cu–Nd bonding with regard to hole conductivity, thus allowing us to restrict the field of interest to the $CuNdO_2$ species, investigated in a forthcoming paper.

Acknowledgements

The authors gratefully acknowledge the Research Council of Norway for the financial support (project number 143421/DESEMAT) and for the computer time at the Norwegian supercomputer facilities. We thanks Dr Smagul Karazhanov for the fruitful discussion on the effective mass calculations.

References

1 H. Kawazoe, H. Yasakuwa, H. Hyodo, M. Kurita, H. Yanagi and H. Hosono, *Nature*, 1997, **389**, 939.
2 M. Snure and A. Tiwari, *Appl. Phys. Lett.*, 2007, **91**, 092123.
3 A. Buljan, P. Alemany and E. Ruiz, *J. Phys. Chem. B*, 1999, **103**, 8060.
4 B. J. Ingram, T. O. Mason, R. Asahi, K. T. Park and A. J. Freeman, *Phys. Rev. B: Condens. Matter Mater. Phys.*, 2001, **64**, 155114.

5 B. J. Ingram, G. B. Gonzalez, T. O. Mason, D. Y. Shahriari, A. Barnabe, D. Ko and K. R. Poeppelmeier, *Chem. Mater.*, 2004, **16**, 5616.
6 D. Kim, S. Park, E. Jeong, H. Lee and S. Choi, *Thin Solid Films*, 2007, **515**, 5103.
7 J. Tate, H. L. Ju, J. C. Moon, A. Zakutayev, A. P. Richard, J. Russell and D. H. McIntyre, *Phys. Rev. B: Condens. Matter Mater. Phys.*, 2009, **80**, 165206.
8 R.-S. Yu, S.-C. Liang, C.-J. Lu, D.-C. Tasi and F.-S. Shieu, *Appl. Phys. Lett.*, 2007, **90**, 191117.
9 J. Tate, M. Jayaraj, A. Draeseke, T. Ulbrich, A. Sleight, K. Vanaja, R. Nagarajan, J. Wager and R. Hoffman, *Thin Solid Films*, 2002, **411**, 119.
10 M. Sasaki and M. Shimode, *J. Phys. Chem. Solids*, 2003, **64**, 1675.
11 C. W. Teplin, T. Kaydanova, D. L. Young, J. D. Perkins, D. S. Ginley, A. Ode and D. W. Readey, *Appl. Phys. Lett.*, 2004, **85**, 3789.
12 N. Duan, A. W. Sleight, M. K. Jayaraj and J. Tate, *Appl. Phys. Lett.*, 2000, **77**, 1325.
13 R. Nagarajan, N. Duan, M. Jayaraj, J. Li, K. Vanaja, A. Yokochi, A. Draeseke, J. Tate and A. Sleight, *Int. J. Inorg. Mater.*, 2001, **3**, 265.
14 B. J. Ingram, B. J. Harder, N. W. Hrabe, T. O. Mason and K. R. Poeppelmeier, *Chem. Mater.*, 2004, **16**, 5623.
15 R. Kykyneshi, B. C. Nielsen, J. Tate, J. Li and A. W. Sleight, *J. Appl. Phys.*, 2004, **96**, 6188.
16 J. Li, A. F. Yokochi and A. W. Sleight, *Solid State Sci.*, 2004, **6**, 831.
17 Y. Kakehi, K. Satoh, T. Yotsuya, A. Ashida, T. Yoshimura and N. Fujimura, *Thin Solid Films*, 2008, **516**, 5785.
18 Y. Kakehi, K. Satoh, T. Yoshimura, A. Ashida and N. Fujimura, *Vacuum*, 2009, **84**, 618.
19 R. Nagarajan, A. D. Draeseke, A. W. Sleight and J. Tate, *J. Appl. Phys.*, 2001, **89**, 8022.
20 T. Arnold, D. J. Payne, A. Bourlange, J. P. Hu, R. G. Egdell, L. F. J. Piper, L. Colakerol, A. De Masi, P.-A. Glans and T. Learmonth, *et al.*, *Phys.Rev. B: Condens. Matter Mater. Phys.*, 2009, **79**, 075102.
21 W. C. Sheets, E. S. Stampler, M. I. Bertoni, M. Sasaki, T. J. Marks, T. O. Mason and K. R. Poeppelmeier, *Inorg. Chem.*, 2008, **47**, 2696.
22 F. A. Benko and F. P. Koffyberg, *Phys. Status Solidi A*, 1986, **94**, 231.
23 M. A. Marquardt, N. A. Ashmore and D. P. Cann, *Thin Solid Films*, 2006, **496**, 146.
24 K. A. Vanaja, R. S. Ajimsha, A. S. Asha and M. K. Jayaraj, *Appl. Phys. Lett.*, 2006, **88**, 212103.
25 H. C. Kandpal and R. Seshadi, *Solid State Sci.*, 2002, **4**, 1045.
26 M. Jansen, *Angew. Chem., Int. Ed.*, 2003, **26**, 1098.
27 F. Benko and F. Koffyberg, *J. Phys. Chem. Solids*, 1987, **48**, 431.
28 X. Nie, S.-H. Wei and S. B. Zhang, *Phys. Rev. Lett.*, 2002, **88**, 066405.
29 K. G. Godinho, B. J. Morgan, J. P. Allen, D. O. Scanlon and G. W. Watson, *J. Phys.: Condens. Matter*, 2011, **23**, 334201.
30 M. N. Huda, Y. Yan, A. Walsh, S.-H. Wei and M. M. Al-Jassim, *Appl. Phys. Lett.*, 2009, **94**, 251907.
31 M. N. Huda, Y. Yan, A. Walsh, S.-H. Wei and M. M. Al-Jassim, *Phys. Rev. B: Condens. Matter Mater. Phys.*, 2009, **80**, 035205.
32 M. N. Huda, Y. Yan and M. M. Al-Jassim, *J. Appl. Phys.*, 2011, **109**, 113710.
33 D. O. Scanlon, A. Walsh, B. J. Morgan, G. W. Watson, D. J. Payne and R. G. Egdell, *Phys. Rev. B: Condens. Matter Mater. Phys.*, 2009, **79**, 035101.
34 D. O. Scanlon and G. W. Watson, *J. Mater. Chem.*, 2011, **21**, 3655.
35 D. O. Scanlon, K. G. Godinho, B. J. Morgan and G. W. Watson, *J. Chem. Phys.*, 2010, **132**, 024707.
36 D. O. Scanlon and G. W. Watson, *J. Phys. Chem. Lett.*, 2010, **1**, 3195.
37 D. O. Scanlon, A. Walsh and G. W. Watson, *Chem. Mater.*, 2009, **21**, 4568.
38 S. Heyd, G. Scuseria and M. Ernzerhof, *J. Chem. Phys.*, 2003, **118**, 8207.
39 R. Gillen and J. Robertson, *Phys. Rev. B: Condens. Matter Mater. Phys.*, 2011, **84**, 035125.
40 J. Robertson, R. Gillen and S. Clark, *Thin Solid Films*, 2012, **520**, 3714.
41 D. M. Bylander and L. Kleinman, *Phys. Rev. B: Condens. Matter Mater. Phys.*, 1990, **41**, 7868.
42 F. Trani, J. Vidal, S. Botti and M. A. L. Marques, *Phys. Rev. B: Condens. Matter Mater. Phys.*, 2010, **82**, 085115.
43 H. Dixit, R. Saniz, S. Cottenier, D. Lamoen and B. Partoens, *J. Phys.: Condens. Matter*, 2012, **24**, 205503.
44 O. K. Andersen, *Phys. Rev. B: Solid State*, 1975, **12**, 3060.
45 S. Kumar and H. Gupta, *Comput. Theor. Chem.*, 2011, **977**, 78.
46 J. P. Perdew, K. Burke and M. Ernzerhof, *Phys. Rev. Lett.*, 1996, **77**, 3865.
47 G. Kresse and J. Furthmller, *Phys. Rev. B: Condens. Matter Mater. Phys.*, 1996, **54**, 11169.
48 G. Kresse and D. Joubert, *Phys. Rev. B: Condens. Matter Mater. Phys.*, 1999, **59**, 1758.
49 P. E. Blochl, *Phys. Rev. B: Condens. Matter Mater. Phys.*, 1994, **50**, 17953.
50 P. Ravindran, R. Vidya, A. Kjekshus, H. Fjellvaag and O. Eriksson, *Phys. Rev. B: Condens. Matter Mater. Phys.*, 2006, **74**, 224412.
51 R. Seshadri, C. Felser, K. Thieme and W. Tremel, *Chem. Mater.*, 1998, **10**, 2189.
52 D. Shin, J. S. Foord, D. J. Payne, T. Arnold, D. J. Aston, R. G. Egdell, K. G. Godinho, D. O. Scanlon, B. J. Morgan and G. W. Watson, *et al.*, *Phys. Rev. B: Condens. Matter Mater. Phys.*, 2009, **80**, 233105.
53 G. Hautier, A. Miglio, G. Ceder, G. Rignanese and X. Gonze, *Nat. Commun.*, 2013, **4**, 2292.
54 H. Yanagi, T. Hase, S. Ibuki, K. Ueda and H. Hosono, *Appl. Phys. Lett.*, 2001, **78**, 1583.
55 T. Otabe, K. Ueda, A. Kudoh, H. Hosono and H. Kawazoe, *Appl. Phys. Lett.*, 1998, **72**, 1036.
56 J. P. Allen, D. O. Scanlon and G. W. Watson, *Phys. Rev. B: Condens. Matter Mater. Phys.*, 2011, **84**, 115141.

57 G. Dong, M. Zhang, M. Wang, F. Tang, H. Li, A. Huang and H. Yan, *J. Phys. Chem. Solids*, 2012, **73**, 1170.
58 G. Brachtel and M. Jansen, *Cryst. Struct. Commun.*, 1981, **10**, 173.
59 T. Ishiguro, A. Kitazawa and M. Kato, *J. Solid State Chem.*, 1981, **40**, 170.
60 B. Koehler and M. Jansen, *Z. Anorg. Allg. Chem.*, 1986, **543**, 73.
61 M. Shimode, M. Sasaki and K. Mukaida, *J. Solid State Chem.*, 2000, **151**, 16.
62 R. Shannon, D. Rogers and C. Prewitt, *Inorg. Chem.*, 1971, **10**, 713.
63 B. Koehler and M. Jansen, *J. Solid State Chem.*, 1987, **71**, 566.
64 J. Pellicer-Porres, A. Segura, A. Gilliland, A. Munoz, P. Rodriguez-Hernendez, D. Kim, M. Lee and T. Kim, *Appl. Phys. Lett.*, 2006, **88**, 181904.
65 S. Gilliland, J. Pellicer-Porres, A. Segura, A. Muoz, P. Rodrguez-Hernndez, D. Kim, M. S. Lee and T. Y. Kim, *Phys. Status Solidi B*, 2007, **244**, 309.
66 K. Ueda, T. Hase, H. Yanagi, H. Kawazoe, H. Hosono, H. Ohta, M. Orita and M. Hirano, *J. Appl. Phys.*, 2001, **89**, 1790.
67 M. Sasaki and M. Shimode, *J. Phys. Chem. Solids*, 2003, **64**, 1675.
68 S. Ouyang, N. Kikugawa, D. Chen, Z. Zou and J. Ye, *J. Phys. Chem. C*, 2009, **113**, 1560.
69 Y. Maruyama, H. Irie and K. Hashimoto, *J. Phys. Chem. B*, 2006, **110**, 23274.